

# A relativistic framework to determine the nuclear transparency from $A(p, 2p)$ reactions

B. Van Overmeire, J. Ryckebusch

*Department of Subatomic and Radiation Physics, Ghent University,  
Proeftuinstraat 86, B-9000 Gent, Belgium*

---

## Abstract

A relativistic framework for computing the nuclear transparency extracted from  $A(p, 2p)$  scattering processes is presented. The model accounts for the initial- and final-state interactions (IFSI) within the relativistic multiple-scattering Glauber approximation (RMSGGA). For the description of color transparency, two existing models are used. The nuclear filtering mechanism is implemented as a possible explanation for the oscillatory energy dependence of the transparency. Results are presented for the target nuclei  ${}^7\text{Li}$ ,  ${}^{12}\text{C}$ ,  ${}^{27}\text{Al}$ , and  ${}^{63}\text{Cu}$ . An approximated, computationally less intensive version of the RMSGGA framework is found to be sufficiently accurate for the calculation of the nuclear transparency. After including the nuclear filtering and color transparency mechanisms, our calculations are in acceptable agreement with the data.

*Key words:*  $A(p, 2p)$  transparency, Glauber theory, color transparency, nuclear filtering

*PACS:* 13.75.Cs, 13.85.Dz, 25.40.Ve, 11.80.La

---

## 1 Introduction

The transition region between nucleon-meson (hadronic) and quark-gluon (partonic) degrees of freedom is a topic of longstanding interest in nuclear physics. A promising observable to map this transition is the transparency of the nuclear medium to the propagation of hadrons. In  $A(p, 2p)$  experiments, the nuclear transparency is defined as the ratio of the cross section per nucleon to the hydrogen one. Accordingly, the nuclear transparency is a measure

---

*Email address:* `Bart.VanOvermeire@UGent.be` (B. Van Overmeire).

for the attenuation effects of the spectator nucleons on the impinging and outgoing protons.

In the conventional Glauber picture [1], the nuclear transparency extracted from  $A(p, 2p)$  reactions is predicted to be rather constant for incoming momentum larger than a few GeV/c. The color transparency (CT) phenomenon suggests an anomalously large transmission probability of protons through nuclei [2,3] and leads to a nuclear transparency that increases with incoming momentum. The experimental  $A(p, 2p)$  data [4,5,6] suggest a CT-like increase in the transparency for impinging proton momenta between 5 and 10 GeV/c. For higher momenta the nuclear transparency falls back to the Glauber level. This oscillatory energy dependence is not unique to the  $A(p, 2p)$  nuclear transparency: it has been observed or hinted at in  $pp$  elastic scattering [7], elastic  $\pi p$  fixed-angle scattering [8,9], pion photoproduction [9,10], and deuteron photodisintegration [11,12].

One possible interpretation of this energy dependence of the  $A(p, 2p)$  transparency is provided by the presence of two terms in the free  $pp$  scattering amplitude [13,14]. Ralston and Pire [13] suggested a combination of the following two components. First, the quark-counting component which follows the dimensional scaling law [15] and represents a small object (a point-like configuration, PLC). Second, the Landshoff component [16] which is associated with normal-sized configurations. The interference between these two amplitudes induces the oscillation of the  $pp$  cross section about the scaling behavior. Inside the nuclear medium, the Landshoff component will be suppressed because of the strong interactions with the spectator nucleons, while the quark-counting component will escape the nucleus with relatively small attenuation due to CT. This phenomenon is called “nuclear filtering” (NF) [17]: the nucleus filters away the normal-sized components in the hadron wave functions. Accordingly, the nucleus plays an active role in selecting small-sized components. The NF model is able to reproduce qualitatively the observed bump in the  $A(p, 2p)$  transparency.

Recently, a relativistic and cross-section factorized framework for  $A(p, 2p)$  reactions has been proposed [18]. In this Letter, this formalism is extended to incorporate the Ralston-Pire model for the  $pp$  scattering amplitude and the concepts of CT and NF. For the description of the initial- and final-state interactions (IFSI) of the impinging and two outgoing protons, we adopt the relativistic multiple-scattering Glauber approximation (RMSGGA) [18]. This relativistic extension of the Glauber model, which was originally developed to describe  $A(e, e'p)$  observables [19,20], models the IFSI as consecutive cumulative scatterings with the individual spectator nucleons in the nucleus. To compute the effects of CT, we consider the quantum diffusion model of Ref. [21] and an alternative treatment presented in Ref. [22]. The comparison between the two CT models is made in a consistent way.

This Letter is organized as follows. In Section 2, the RMSGA  $A(p, 2p)$  formalism of Ref. [18] is extended to take into account both the quark-counting and the Landshoff contribution to the hard  $pp$  scattering amplitude. A numerically convenient approximate form of the RMSGA framework is introduced. Further, we describe two different methods to deal with CT, thereby indicating the similarities and differences. Section 3 presents the nuclear transparency results for the target nuclei  ${}^7\text{Li}$ ,  ${}^{12}\text{C}$ ,  ${}^{27}\text{Al}$ , and  ${}^{63}\text{Cu}$ . The effect of IFSI, CT and NF is discussed. Furthermore, the accuracy of the approximated RMSGA approach is investigated and the two CT treatments are compared. Finally, Section 4 summarizes our findings and states our conclusions.

## 2 Formalism

In the Ralston-Pire approach [23], the spin-averaged  $pp$  scattering amplitude consists of the quark-counting (QC) and the Landshoff (L) contribution:

$$\mathcal{M}^{pp} = \mathcal{M}_{\text{QC}}^{pp} + \mathcal{M}_{\text{L}}^{pp} . \quad (1)$$

The  $\mathcal{M}_{\text{QC}}^{pp}$  term results in a differential cross section that scales like  $d\sigma^{pp}/dt \propto s^{-10}$  and the Landshoff term can be related to it through

$$\mathcal{M}_{\text{L}}^{pp} = \frac{\rho_1}{2} \sqrt{\frac{s}{1 \text{ GeV}^2}} e^{\pm i(\phi(s)+\delta_1)} \mathcal{M}_{\text{QC}}^{pp} . \quad (2)$$

Here,  $s$  and  $t$  are the Mandelstam variables. Further,  $\rho_1 = 0.08$ ,  $\phi(s) = \frac{\pi}{0.06} \ln \left\{ \ln \left[ \frac{s}{0.01 \text{ GeV}^2} \right] \right\}$ , and  $\delta_1 = -2.0$ . These values were determined from a fit to the  $pp$  data at  $90^\circ$  [23]. The sole parameter which remains undetermined is the sign of the phase difference  $\phi(s) + \delta_1$  between the quark-counting and the Landshoff term. Therefore, both signs will be used in the calculations.

Incorporating the Ralston-Pire approach and the NF mechanism into the  $A(p, 2p)$  formalism of Ref. [18], the amplitude for the  $p(E_{p1}, \vec{p}_1, m_{s1i}) + A(E_A, \vec{k}_A, 0^+) \rightarrow p(E_{k1}, \vec{k}_1, m_{s1f}) + p(E_{k2}, \vec{k}_2, m_{s2f}) + A-1(E_{A-1}, \vec{k}_{A-1}, J_R M_R)$  reaction becomes

$$\begin{aligned} \mathcal{M}_{fi}^{(p,2p)} = & \sum_{m_s} \left( \mathcal{M}_{\text{QC}}^{pp} \right)_{m_{s1i}, m_s, m_{s1f}, m_{s2f}} \bar{u}(\vec{p}_m, m_s) \phi_{\alpha_1}^{\text{RMSGGA+CT}}(\vec{p}_m) \\ & + \sum_{m_s} \left( \mathcal{M}_{\text{L}}^{pp} \right)_{m_{s1i}, m_s, m_{s1f}, m_{s2f}} \bar{u}(\vec{p}_m, m_s) \phi_{\alpha_1}^{\text{RMSGGA}}(\vec{p}_m) , \end{aligned} \quad (3)$$

where  $\vec{p}_m = \vec{k}_1 + \vec{k}_2 - \vec{p}_1$  is the missing momentum and  $\alpha_1$  refers to the state wherein the struck proton resided. In this expression, the effect of IFSI is ac-

counted for through the distorted momentum-space wave functions  $\phi_{\alpha_1}^{\text{RMSGGA+CT}}(\vec{p}_m)$  and  $\phi_{\alpha_1}^{\text{RMSGGA}}(\vec{p}_m)$ . Since the quark-counting term is associated with PLCs, the corresponding momentum-space wave function  $\phi_{\alpha_1}^{\text{RMSGGA+CT}}(\vec{p}_m)$  includes the effect of CT. The Landshoff term, on the other hand, corresponds with a hadron of normal size. Consequently, the IFSI can be computed in standard Glauber theory. Using the spin-averaged  $pp$  matrix element of Eq. (1), the squared  $A(p, 2p)$  matrix element for knockout from the  $\alpha_1$  shell can be cast in the form

$$\begin{aligned} \overline{\sum_{if}} |\mathcal{M}_{fi}^{(p,2p)}|^2 = & \sum_{m, m_s} \left\{ |\mathcal{M}_{\text{QC}}^{pp}|^2 \left| \bar{u}(\vec{p}_m, m_s) \phi_{\alpha_1}^{\text{RMSGGA+CT}}(\vec{p}_m) \right|^2 \right. \\ & + 2\text{Re} \left[ \mathcal{M}_{\text{QC}}^{pp} (\mathcal{M}_{\text{L}}^{pp})^* \bar{u}(\vec{p}_m, m_s) \phi_{\alpha_1}^{\text{RMSGGA+CT}}(\vec{p}_m) \right. \\ & \quad \left. \left. \times \left( \bar{u}(\vec{p}_m, m_s) \phi_{\alpha_1}^{\text{RMSGGA}}(\vec{p}_m) \right)^* \right] \right. \\ & \left. + |\mathcal{M}_{\text{L}}^{pp}|^2 \left| \bar{u}(\vec{p}_m, m_s) \phi_{\alpha_1}^{\text{RMSGGA}}(\vec{p}_m) \right|^2 \right\}, \end{aligned} \quad (4)$$

with  $m$  the struck nucleon's generalized angular momentum quantum number. The differential cross section is obtained as an incoherent sum of the squared matrix elements over all proton levels  $\alpha_1$ , thereby factoring in the occupation number of every level. The momentum-space wave function is defined as [18]

$$\phi_{\alpha_1}^{\text{RMSGGA(+CT)}}(\vec{p}_m) = \int d\vec{r} e^{-i\vec{p}_m \cdot \vec{r}} \phi_{\alpha_1}(\vec{r}) \widehat{\mathcal{S}}_{\text{IFSI}}^{\text{RMSGGA(+CT)}}(\vec{r}), \quad (5)$$

where the relativistic bound-state wave function  $\phi_{\alpha_1}(\vec{r})$  is computed in the Hartree approximation to the  $\sigma - \omega$  model [24], using the W1 parametrization for the different field strengths [25]. The  $\widehat{\mathcal{S}}_{\text{IFSI}}^{\text{RMSGGA(+CT)}}(\vec{r})$  operator accounts for the IFSI effects and is the subject of the forthcoming discussion. Hereafter, results obtained on the basis of Eq. (4) are dubbed RMSGA+CT+NF.

In the RMSGA framework, the IFSI operator takes on the form [18]

$$\begin{aligned} \widehat{\mathcal{S}}_{\text{IFSI}}^{\text{RMSGGA}}(\vec{r}) = & \prod_{j=2}^A \left\{ \int d\vec{r}_j \left| \phi_{\alpha_j}(\vec{r}_j) \right|^2 \left[ 1 - \Gamma_{pN}(p_1, \vec{b} - \vec{b}_j) \theta(z - z_j) \right] \right. \\ & \times \left[ 1 - \Gamma_{pN}(k_1, \vec{b}' - \vec{b}_j') \theta(z_j' - z') \right] \\ & \left. \times \left[ 1 - \Gamma_{pN}(k_2, \vec{b}'' - \vec{b}_j'') \theta(z_j'' - z'') \right] \right\}, \end{aligned} \quad (6)$$

where  $\vec{r}$  denotes the point of collision between the struck and incoming proton, and  $\vec{r}_j$  ( $j = 2, \dots, A$ ) are the positions of the frozen spectator nucleons. Further, the  $z$  axis lies along  $\vec{p}_1$ ,  $z'$  along  $\vec{k}_1$ , and  $z''$  along  $\vec{k}_2$ . The  $\vec{b}$ ,  $\vec{b}'$ , and  $\vec{b}''$

planes are perpendicular to these proton momenta. Reflecting the diffractive nature of  $pN$  collisions at GeV energies, the profile function for  $pN$  scattering is parametrized as

$$\Gamma_{pN}(k, \vec{b}) = \frac{\sigma_{pN}^{\text{tot}}(k)(1 - i\epsilon_{pN}(k))}{4\pi(\beta_{pN}(k))^2} \exp\left(-\frac{\vec{b}^2}{2(\beta_{pN}(k))^2}\right). \quad (7)$$

The total  $pN$  cross section  $\sigma_{pN}^{\text{tot}}(k)$ , the slope parameter  $\beta_{pN}(k)$ , and the ratio of the real to the imaginary part of the scattering amplitude  $\epsilon_{pN}(k)$  depend on the proton momentum  $k$ . In the numerical calculations, their values are obtained through interpolation of the  $NN$  scattering database from the Particle Data Group [26].

Eq. (6) is a genuine  $A$ -body operator and the integration over the coordinates of the spectator nucleons makes its numerical evaluation very challenging. The IFSI operator can be rewritten in a numerically more convenient form by adopting the following approximations. First, the squared wave functions of the spectator protons (neutrons) are replaced by  $1/(Z-1)$  ( $1/N$ ) times the proton (neutron) density of the residual nucleus. Second, one assumes that these densities are slowly varying functions of  $\vec{b}$ , while  $\Gamma_{pN}(k, \vec{b})$  is sharply peaked at  $\vec{b} = \vec{0}$ . This allows one to approximate the IFSI operator of Eq. (6) by the one-body operator [27]:

$$\begin{aligned} \widehat{\mathcal{S}}_{\text{IFSI}}^{\text{RMSGGA}'}(\vec{r}) &= \prod_{N=p,n} e^{-\frac{1}{2}\sigma_{pN}^{\text{tot}}(p_1)(1-i\epsilon_{pN}(p_1))} \int_{-\infty}^z dz_j \rho_N(\vec{b}, z_j) \\ &\times e^{-\frac{1}{2}\sigma_{pN}^{\text{tot}}(k_1)(1-i\epsilon_{pN}(k_1))} \int_{z'}^{+\infty} dz_j' \rho_N(\vec{b}', z_j') \\ &\times e^{-\frac{1}{2}\sigma_{pN}^{\text{tot}}(k_2)(1-i\epsilon_{pN}(k_2))} \int_{z''}^{+\infty} dz_j'' \rho_N(\vec{b}'', z_j''). \end{aligned} \quad (8)$$

Here,  $\rho_p$  and  $\rho_n$  are the proton and neutron density of the residual nucleus. They reflect the spatial distribution of the scattering centers inside this nucleus. Henceforth, calculations based on Eq. (8) are labeled as RMSGA'.

The essential assumption of CT is that the impinging proton compresses to a PLC as it hits a target nucleon, after which the outgoing protons expand from PLCs to normal-sized objects as they move through the nucleus. To account for the reduced interaction of a PLC with the nuclear medium, the total cross sections  $\sigma_{pN}^{\text{tot}}$  in Eqs. (7) and (8) are replaced by effective ones. In the partonic model of Farrar et al. [21] (denoted by FLFS), the interaction cross section is argued to be

$$\sigma_{pN}^{\text{FLFS}}(p, Z) = \sigma_{pN}^{\text{tot}} \left\{ \left[ \frac{Z}{l_h} + \frac{\langle n^2 k_t^2 \rangle}{|t|} \left(1 - \frac{Z}{l_h}\right) \right] \theta(l_h - Z) + \theta(Z - l_h) \right\}. \quad (9)$$

Here,  $Z$  is the distance from the hard interaction point along the trajectory of the particle,  $n = 3$  is the number of constituents in the proton, and  $\langle k_t^2 \rangle^{1/2} = 0.35$  GeV/c is the average transverse momentum of a parton in a hadron. The quantity  $l_h \simeq 2p/\Delta M^2$  is the hadronic expansion length, i.e., the propagation distance at which an expanding hadron reaches its normal hadronic size, and depends on the hadron momentum  $p$  and the squared mass difference  $\Delta M^2$  between the intermediate PLC and the normal-sized hadron. It is commonly assumed that  $0.7 \leq \Delta M^2 \leq 1.1$  (GeV/c<sup>2</sup>)<sup>2</sup> are reasonable values.

Starting from a hadronic picture, Jennings and Miller [22] suggested the following alternative expression for the effective cross section

$$\sigma_{pN}^{\text{JM}}(p, Z) = \sigma_{pN}^{\text{tot}} \left( 1 - \frac{p}{p^*} e^{i(p-p^*)Z} \right), \quad (10)$$

with  $p$  the proton momentum and  $p^*$  the momentum of a baryon resonance with a complex mass  $M^*$  and the same energy as the nucleon, i.e.,  $(p^*)^2 = p^2 + M_p^2 - (M^*)^2$ . The expression for the effective cross section emanates from the intermediate PLC being a superposition of the nucleon ground state and a nucleon resonance. The imaginary part of  $M^*$  ensures the decay of the intermediate state to an asymptotically free, normal-sized proton. Like the FLFS approach of Eq. (9), Eq. (10) considers one excited state in the PLC. It is worth noting that both the FLFS and JM model take into account the suppression of interaction in the collision point and the time evolution of the PLC to a normal-sized proton during its propagation through the nucleus.

In our numerical calculations, we will also consider the standard RMSGA+CT picture. In this scenario, the entire wave packet of the incoming and outgoing protons is assumed to be in a PLC, which propagates through a passive nuclear medium. This amounts to neglecting the Landshoff term in the amplitudes  $\mathcal{M}^{pp}$  and  $\mathcal{M}_{fi}^{(p,2p)}$  of Eqs. (1) and (3). Finally, in the standard RMSGA calculations, both the Landshoff term and CT effects are neglected.

For the free  $pp$  scattering cross section  $d\sigma^{pp}/dt$ , the parametrization as presented in Ref. [28] is used. This parametrization combines the  $\theta_{c.m.}$  dependence suggested by [29] and the Ralston-Pire separation of Eq. (2).

### 3 Nuclear transparency results

The nuclear transparency is computed as the ratio of the cross sections including and excluding IFSI effects:

$$T = \frac{\sigma^{(p,2p)}}{\sigma_{\text{RPWIA}}^{(p,2p)}} . \quad (11)$$

The relativistic plane wave approximation (RPWIA) limit is reached by setting the IFSI operator  $\hat{\mathcal{S}}_{\text{IFSI}}(\vec{r})$  equal to one in Eq. (5), and corresponds with a calculation which ignores IFSI. The numerator and denominator of Eq. (11) are obtained by integrating the corresponding differential cross sections over the phase space defined by the kinematic cuts. In our calculations, we adopted identical cuts as in the experiments [4,5,6] and assumed a flat experimental acceptance within the kinematical ranges for each data point.

We consider the experimental nuclear transparency values as presented in [30]. The incident lab momentum varies from 5.9 to 14.4 GeV/c and the scattering angle is near  $90^\circ$  in the  $pp$  center of mass. The Mandelstam variable  $|t| \simeq (s - 4M_p^2)/2$  extends from 4.7 to 12.7 (GeV/c)<sup>2</sup>. In Ref. [30], the originally published values of Carroll et al. [4] were rescaled using the improved nuclear momentum distributions of Ref. [31], thereby making them consistent with the data of Refs. [5,6].

First, we address the energy dependence of the  $^{12}\text{C}(p, 2p)$  transparency and study the role of IFSI, CT and NF. Further, we use the  $^{12}\text{C}(p, 2p)$  calculations as a test case to determine the accuracy of the IFSI operator of Eq. (8) relative to the expression of Eq. (6). Fig. 1 displays the  $^{12}\text{C}$  transparency as a function of the incoming proton momentum  $p_1$ . The solid curves represent the full RMSGA calculations, whereas the RMSGA' results are shown as dashed curves. Three different scenarios were considered. As expected, the standard RMSGA calculations lead to a nuclear transparency that is almost independent of the beam momentum. The main effect of the IFSI is to reduce the nuclear transparency from the asymptotic value of 1 to  $\sim 0.15$ . The inclusion of CT effects produces a transparency linearly rising with energy. The increase relative to the RMSGA result is highly dependent on the adopted model and corresponding parameters for CT. The curves including CT shown in Fig. 1 adopt the FLFS model with  $\Delta M^2 = 0.7$  (GeV/c<sup>2</sup>)<sup>2</sup>. The increase of the transparency is consistent with the data in the range 5–10 GeV/c, but the RMSGA+CT picture fails to explain the drop in the transparency at higher momenta. Our RMSGA and RMSGA+CT predictions confirm the results of [32]. A better agreement with the data is obtained when adding the mechanism of NF. Compared to the RMSGA+CT results, the transparency is increased

at intermediate momenta (5–10 GeV/c) and decreased at higher momenta, two effects which improve the description of the data. A similar result was obtained in Ref. [33] where the JM model of CT was used.

Concerning the comparison of the RMSGA and RMSGA' results, it can be inferred from Fig. 1 that both approaches yield nearly identical results which differ at the 2–3% level. Consequently, the operator of Eq. (8) is considered sufficiently accurate for the calculation of the nuclear transparency and will be used in the remainder of this work. We wish to stress that the computational cost of Eq. (8) is about a factor of  $10^3$  lower than the full-blown RMSGA operator of Eq. (6).

Figs. 2 and 3 are devoted to a comparison of the different CT models. Results of the FLFS quantum diffusion model are plotted for  $\Delta M^2 = 0.7$  and  $1.1$  (GeV/c<sup>2</sup>)<sup>2</sup>. For the  $M^*$  parameter of the JM model we consider three different values, representing the  $\Delta$ , the Roper resonance, and the average of the lowest  $P$ -wave  $N^*$  resonances. For the imaginary part of  $M^*$  a value of 150 MeV was taken. The lowest values of the parameters  $\Delta M^2$  and  $M^*$  induce the strongest increase of the RMSGA+CT transparency with the beam momentum  $p_1$  and also lead to the largest deviations between the predictions including the NF mechanism and the corresponding RMSGA+CT results.

Fig. 2 shows that after including NF and CT, the calculations correctly reproduce the maximum in the  $^{12}\text{C}(p, 2p)$  transparency at about 9.5 GeV/c, but badly fail to fall back low enough to account for the 14.4 GeV/c data point. Ralston and Pire [13], on the other hand, do succeed in reproducing the maxima and minima in the nuclear transparency data. However, they assume that the transparency of the quark-counting term is beam-energy independent, a rather speculative assumption. The CT-induced increase of the quark-counting transparency with energy causes our RMSGA+CT+NF predictions to rise again at a momentum  $p_1 \simeq 12$  GeV/c.

In the FLFS as well as the JM approach, the RMSGA+CT+NF predictions reproduce the general trend of the data, but no variant achieves very good agreement. Furthermore, it is not possible to unambiguously determine the value of the parameters  $\Delta M^2$  and  $M^*$ , as the best choice for these parameters depends on the target nucleus under consideration. Fig. 2 suggests that for the  $^{12}\text{C}(p, 2p)$  reaction  $M^* = (1440 + 150i)$  MeV leads to the best agreement, while for the  $\Delta M^2$  parameter no “best” choice can be put forward. Fig. 3, on the other hand, shows that for the  $^{27}\text{Al}$  target nucleus the FLFS results are systematically below the data in the region below 10 GeV/c. Using  $M^* = (1440 + 150i)$  MeV in the JM model also does not increase the transparency high enough so as to match the 6 and 10 GeV/c data points, only with  $M^* = (1232 + 150i)$  MeV is the CT-induced increase of the transparency strong enough.

None of the results shown in this Letter include the color screening effect (CSE) [34]. This QCD effect suggests the suppression of the small-size configurations in bound nucleons. We deem that the CT parameters are so badly constrained that controlling additional mechanisms is out of reach for the moment. In both the RMSGA+CT and the RMSGA+CT+NF calculations, the inclusion of the CSE decreases the transparency by 6–12%, with the largest effect occurring at higher  $p_1$ .

Another effect that can be studied in Figs. 2 and 3 is the influence of the sign of  $\phi(s) + \delta_1$  on the RMSGA+CT+NF results. For the FLFS model of CT, the differences between calculations using both signs of  $\phi(s) + \delta_1$  are minor. As already observed by Jennings and Miller [33], the results using the JM model of CT are rather sensitive to this sign. The discrepancy between the FLFS- and JM-based calculations arises from the different structure of the effective cross sections (9) and (10). Indeed, these effective cross sections not only determine the attenuation of the quark-counting term in the nuclear medium, but also the phase difference between the quark-counting and the Landshoff term. Whereas the real parts of both effective cross sections are quite similar, the FLFS effective cross section (9) is purely real, while its JM counterpart also has an imaginary part. This imaginary part causes the enhanced sensitivity of the JM results to the sign of  $\phi(s) + \delta_1$ . As for which sign causes the best agreement with the data, no firm conclusions can be drawn. Indeed, the optimum choice for the sign of  $\phi(s) + \delta_1$  depends on the used CT model (FLFS or JM), the value of the parameter  $\Delta M^2$  or  $M^*$ , and the target nucleus. For the  ${}^7\text{Li}(p, 2p)$  reaction, the positive sign provides the best agreement, while the  ${}^{63}\text{Cu}$  transparency data rather require a negative sign.

The  $A$  dependence of the nuclear transparency at two values of the incoming momentum  $p_1$  is studied in Fig. 4. The standard RMSGA calculations fall considerably below the data. Further, none of the RMSGA+CT+NF calculations succeed in simultaneously describing the data for all target nuclei. While the FLFS approach agrees with the  ${}^7\text{Li}$  and  ${}^{12}\text{C}$  data points rather well using  $\Delta M^2 = 0.7 (\text{GeV}/c^2)^2$ , the FLFS results tend to underestimate the  ${}^{27}\text{Al}$  and  ${}^{63}\text{Cu}$  data. With regard to the  $M^*$  parameter of the JM model, for the  ${}^7\text{Li}$  and  ${}^{12}\text{C}$  nuclei a value of  $M^* = (1440 + 150i)$  MeV seems acceptable, whereas the heavier  ${}^{27}\text{Al}$  and  ${}^{63}\text{Cu}$  nuclei need a smaller  $M^*$  value. A general feature of the RMSGA+CT+NF predictions is that their  $A$  dependence is steeper than the data. Finally, the dot-dashed and dotted curves indicate that the 6 GeV/c data are proportional to  $A^{-2/3}$ , while at 10 GeV/c the  $A$  dependence of the data is more gradual ( $T \propto A^{-1/3}$ ). This trend is not reproduced by the standard RMSGA predictions, which are almost independent of the incoming momentum. When CT and NF effects are included, the softening of the  $A$  dependence with increasing incoming momentum is also present in the calculations. For example, the FLFS calculations with  $\Delta M^2 = 0.7 (\text{GeV}/c^2)^2$  correspond to  $T \propto A^{-0.83}$  at 6 GeV/c incoming momentum and  $T \propto A^{-0.70}$

at 10 GeV/c.

## 4 Conclusions

In conclusion, we have developed a relativistic framework to calculate the nuclear transparency for  $A(p, 2p)$  processes. A relativistic multiple-scattering Glauber model was used to account for the IFSI. To reduce the computational cost of the RMSGA calculations, some additional approximations were made. The predictions with the full and the approximated RMSGA approach agree at the few percent level. Thus, to determine integrated quantities such as the nuclear transparency, a valid alternative for the computationally intensive RMSGA framework is available.

Using the concept of nuclear filtering, our calculations are in qualitative agreement with the data, thereby confirming earlier calculations [33,35,36]. Furthermore, our calculations seem to indicate that CT is imperative to increase the calculations to the level of the data. The same conclusion was reported in Refs. [36,37]. The quantitative description of the data, however, is far from perfect and it is not possible to constrain the magnitude of the parameters in the CT models.

The indications for CT in  $A(p, 2p)$  reactions are not necessarily in contradiction with the results from  $A(e, e'p)$  experiments. Although the  $A(e, e'p)$  transparencies show no significant increase with the four-momentum transfer  $Q^2$  [38] and can be reasonably reproduced in the RMSGA framework, the existence of CT can not be excluded since the predicted effect is small [39]. This is caused by the small expansion times of the PLC to normal size at the present  $A(e, e'p)$  kinematics. The effect of CT is more pronounced in the  $A(p, 2p)$  transparency for different reasons. First, in the  $A(p, 2p)$  reaction there are three particles that can experience CT instead of only one in  $A(e, e'p)$  reactions. Second,  $A(p, 2p)$  data are available up to  $Q^2 = |t|$  values of 12.7 (GeV/c)<sup>2</sup>, while  $A(e, e'p)$  transparency experiments are restricted to  $Q^2 \lesssim 8$  (GeV/c)<sup>2</sup>.

A number of uncertainties involving the  $A(p, 2p)$  transparency remain. One subject of discussion is the size of the Landshoff term. According to Botts et al. [40], this term might also be small-sized. This would make the survival probability of the Landshoff and the quark-counting term rather similar and would weaken the oscillations in the energy dependence of the computed transparencies. Apart from the Ralston-Pire picture discussed above, other explanations of the energy dependence of the transparency have been suggested. For example, Brodsky and de Teramond [14] interpreted the oscillatory behavior in terms of two broad baryon resonances associated with strange and

charmed particle production thresholds, interfering with a perturbative QCD background. An improved set of data, particularly at higher energies, is essential to clarify these issues. The 50 GeV proton synchrotron that is under construction at J-PARC [41] opens great opportunities for this research.

## Acknowledgements

The authors would like to thank M. Sargsian for providing us with the parametrization of the free  $pp$  elastic cross section. This work was supported by the Fund for Scientific Research, Flanders (FWO).

## References

- [1] R.J. Glauber, in: W.E. Brittin, et al. (Eds.), Lectures in Theoretical Physics, Interscience, New York, 1959.
- [2] A.H. Mueller, in: J. Tran Thanh Van (Ed.), Proceedings of the XVII Rencontre de Moriond, Les Arcs, France, Editions Frontières, Gif-sur-Yvette, 1982, p. 13.
- [3] S.J. Brodsky, in: E.W. Kittel, W. Metzger, A. Stergiou (Eds.), Proceedings of the XIII International Symposium on Multiparticle Dynamics, Volendam, The Netherlands, World Scientific, Singapore, 1982, p. 963.
- [4] A.S. Carroll, et al., Phys. Rev. Lett. 61 (1988) 1698.
- [5] I. Mardor, et al., Phys. Rev. Lett. 81 (1998) 5085.
- [6] A. Leksanov, et al., Phys. Rev. Lett. 87 (2001) 212301.
- [7] A.W. Hendry, Phys. Rev. D 10 (1974) 2300.
- [8] D.P. Owen, et al., Phys. Rev. 181 (1969) 1794;  
K.A. Jenkins, et al., Phys. Rev. D 21 (1980) 2445;  
C. Baglin, et al., Nucl. Phys. B 216 (1983) 1;  
J. Blazey, Ph.D. thesis, University of Minnesota, 1986.
- [9] P. Jain, B. Kundu, J.P. Ralston, Phys. Rev. D 65 (2002) 094027.
- [10] L.Y. Zhu, et al., Phys. Rev. Lett. 91 (2003) 022003;  
L.Y. Zhu, et al., Phys. Rev. C 71 (2005) 044603.
- [11] J. Napolitano, et al., Phys. Rev. Lett. 61 (1988) 2530;  
S. J. Freedman, et al., Phys. Rev. C 48 (1993) 1864;  
J. E. Belz, et al., Phys. Rev. Lett. 74 (1995) 646;

- C. Bochna, et al., Phys. Rev. Lett. 81 (1998) 4576;  
 E. C. Schulte, et al., Phys. Rev. Lett. 87 (2001) 102302.
- [12] L.L. Frankfurt, G.A. Miller, M.M. Sargsian, M.I. Strikman, Phys. Rev. Lett. 84 (2000) 3045.
- [13] J.P. Ralston, B. Pire, Phys. Rev. Lett. 61 (1988) 1823.
- [14] S.J. Brodsky, G.F. de Teramond, Phys. Rev. Lett. 60 (1988) 1924.
- [15] S.J. Brodsky, G.R. Farrar, Phys. Rev. Lett. 31 (1973) 1153;  
 S.J. Brodsky, G.R. Farrar, Phys. Rev. D 11 (1975) 1309;  
 V.A. Matveev, R.M. Muradian, A.N. Tavkhelidze, Lett. Nuovo Cimento 7 (1973) 719;  
 G.P. Lepage, S.J. Brodsky, Phys. Rev. D 22 (1980) 2157.
- [16] P.V. Landshoff, Phys. Rev. D 10 (1974) 1024.
- [17] P. Jain, B. Pire, J.P. Ralston, Phys. Rep. 271 (1996) 67.
- [18] B. Van Overmeire, W. Cosyn, P. Lava, J. Ryckebusch, Phys. Rev. C 73 (2006) 064603.
- [19] J. Ryckebusch, D. Debruyne, P. Lava, S. Janssen, B. Van Overmeire, T. Van Cauteren, Nucl. Phys. A 728 (2003) 226.
- [20] P. Lava, M.C. Martínez, J. Ryckebusch, J.A. Caballero, J.M. Udías, Phys. Lett. B 595 (2004) 177.
- [21] G.R. Farrar, H. Liu, L.L. Frankfurt, M.I. Strikman, Phys. Rev. Lett. 61 (1988) 686.
- [22] B.K. Jennings, G.A. Miller, Phys. Rev. D 44 (1991) 692.
- [23] B. Pire, J. P. Ralston, Phys. Lett. B 117 (1982) 233;  
 J. P. Ralston, B. Pire, Phys. Rev. Lett. 49 (1982) 1605.
- [24] B.D. Serot, J.D. Walecka, Adv. Nucl. Phys. 16 (1986) 1.
- [25] R.J. Furnstahl, B.D. Serot, H.-B. Tang, Nucl. Phys. A 615 (1997) 441.
- [26] K. Hagiwara, et al., Phys. Rev. D 66 (2002) 010001, <http://pdg.lbl.gov>.
- [27] C.J. Joachain, C. Quigg, Rev. Mod. Phys. 46 (1974) 279;  
 C.J. Joachain, *Quantum Collision Theory* (Elsevier, Amsterdam, 1975).
- [28] I. Yaron, L.L. Frankfurt, E. Piazzetsky, M. Sargsian, M.I. Strikman, Phys. Rev. C 66 (2002) 024601.
- [29] D. Sivers, S.J. Brodsky, R. Blankenbecler, Phys. Rep. 23 (1976) 1.
- [30] J. Aclander, et al., Phys. Rev. C 70 (2004) 015208.

- [31] C. Ciofi degli Atti, S. Simula, Phys. Rev. C 53 (1996) 1689.
- [32] T.-S.H. Lee, G.A. Miller, Phys. Rev. C 45 (1992) 1863.
- [33] B.K. Jennings, G.A. Miller, Phys. Lett. B 274 (1992) 442.
- [34] L.L. Frankfurt, M.I. Strikman, Nucl. Phys. B 250 (1985) 143;  
L.L. Frankfurt, M.I. Strikman, Phys. Rep. 160 (1988) 235.
- [35] B.K. Jennings, G.A. Miller, Phys. Rev. Lett. 69 (1992) 3619.
- [36] B.K. Jennings, G.A. Miller, Phys. Lett. B 318 (1993) 7.
- [37] P. Jain, J.P. Ralston, Phys. Rev. D 48 (1993) 1104.
- [38] N.C.R. Makins, et al., Phys. Rev. Lett. 72 (1994) 1986;  
T.G. O'Neill, et al., Phys. Lett. B 351 (1995) 87;  
D. Abbott, et al., Phys. Rev. Lett. 80 (1998) 5072;  
K. Garrow, et al., Phys. Rev. C 66 (2002) 044613;  
D. Dutta, et al., Phys. Rev. C 68 (2003) 064603.
- [39] N.N. Nikolaev, A. Szczurek, J. Speth, J. Wambach, B.G. Zakharov, V.R. Zoller, Phys. Rev. C 50 (1994) R1296;  
L.L. Frankfurt, M.I. Strikman, M.B. Zhalov, Phys. Rev. C 50 (1994) 2189;  
L.L. Frankfurt, G.A. Miller, M.I. Strikman, Ann. Rev. Nucl. Part. Sci. 44 (1994) 501.
- [40] J. Botts, G. Sterman, Nucl. Phys. B 325 (1989) 62;  
J. Botts, G. Sterman, Phys. Lett. B 224 (1989) 201;  
J. Botts, G. Sterman, Phys. Lett. B 227 (1989) 501(E);  
J. Botts, Nucl. Phys. B 353 (1991) 20;  
J. Botts, J.-W. Qiu, G. Sterman, Nucl. Phys. A 527 (1991) 577.
- [41] J-PARC home page: <http://j-parc.jp/index-e.html>;  
S. Kumano, hep-ph/0608105.

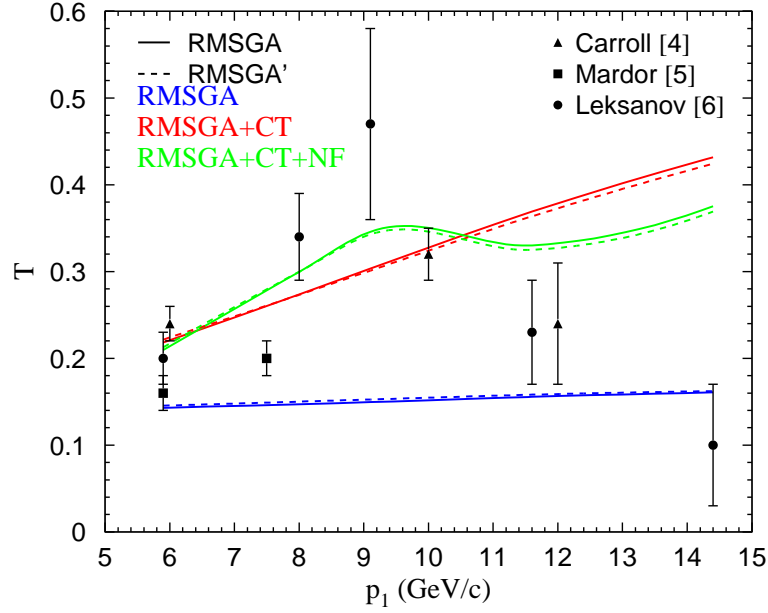


Fig. 1. The nuclear transparency for the  $^{12}\text{C}(p, 2p)$  reaction as a function of the incoming lab momentum  $p_1$ . The full RMSGGA (solid lines) are compared to the RMSGGA' (dashed lines) results. The different curves represent the RMSGGA, RMSGGA+CT and RMSGGA+CT+NF calculations. The CT effects are calculated in the FLFS model [21] with  $\Delta M^2 = 0.7$  (GeV/c<sup>2</sup>)<sup>2</sup> and the results including the mechanism of NF are obtained using the positive sign of  $\phi(s) + \delta_1$ . Data are from Refs. [4,5,6].

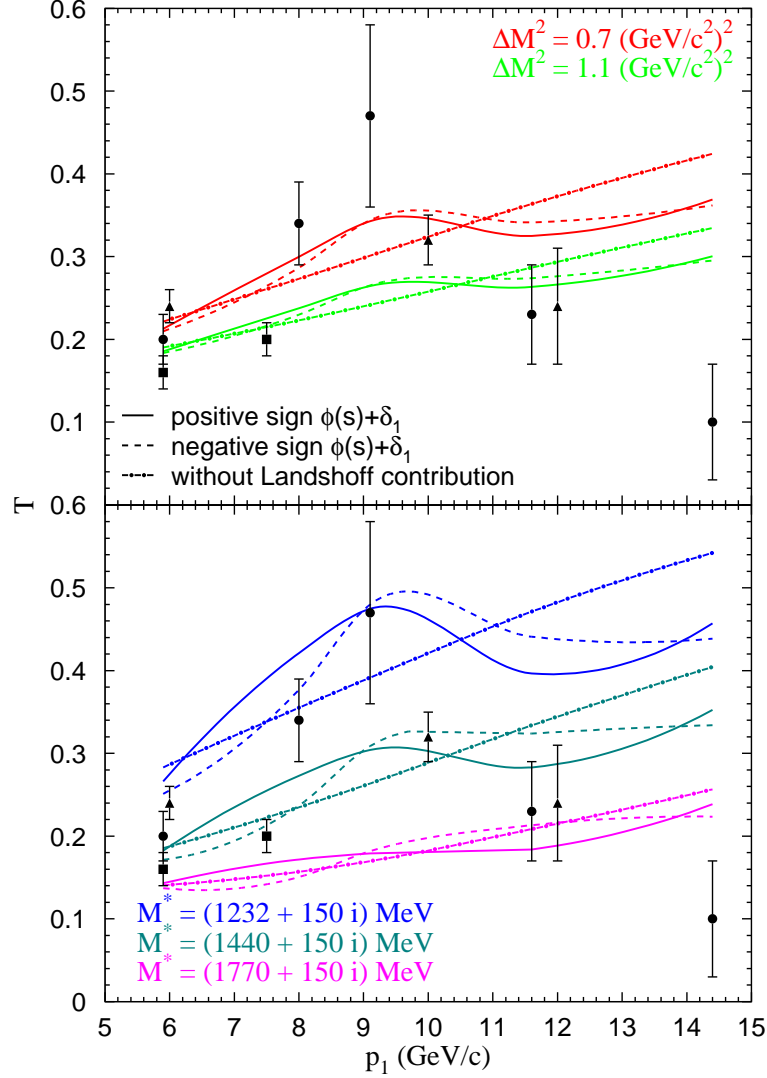


Fig. 2. The  $^{12}\text{C}(p, 2p)$  transparency versus the incoming lab momentum  $p_1$ . The upper (lower) panel depicts results using the FLFS (JM) model for CT. Calculations including the effects of CT and NF with the positive (solid lines) and negative (dashed lines) sign for  $\phi(s) + \delta_1$  are shown, along with the RMSGA+CT predictions (dot-dashed lines). Data are from Refs. [4] (solid triangles), [5] (solid squares), and [6] (solid circles).

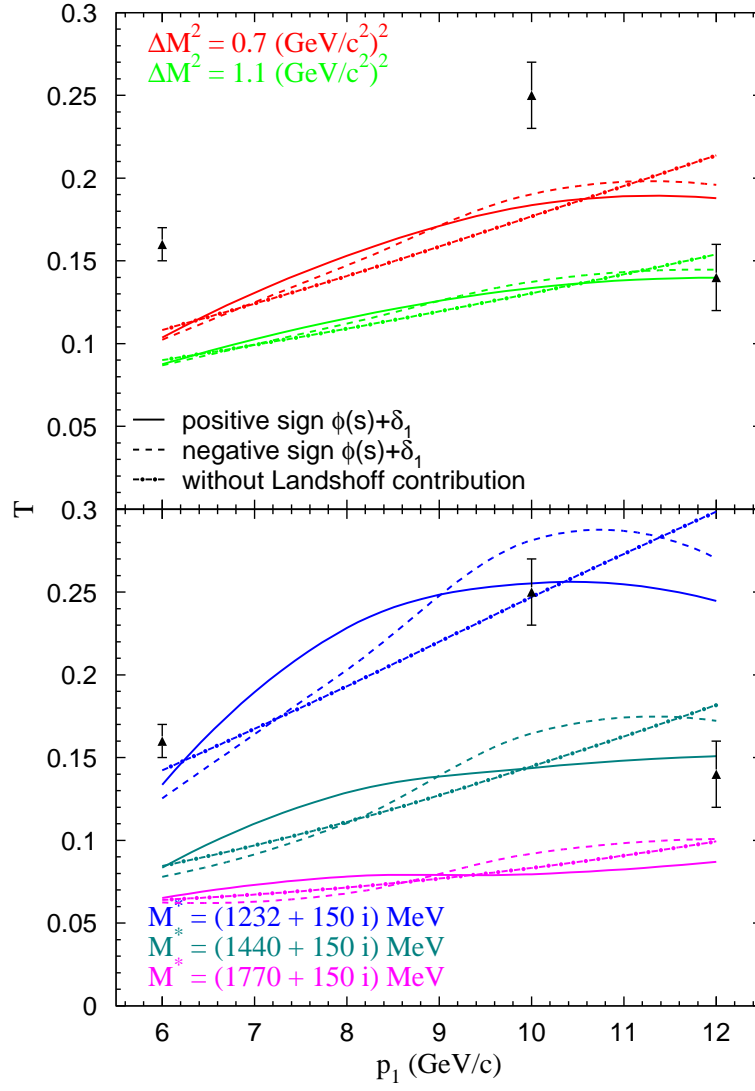


Fig. 3. As in Fig. 2, but for  $^{27}\text{Al}$ . Data are from Ref. [4].

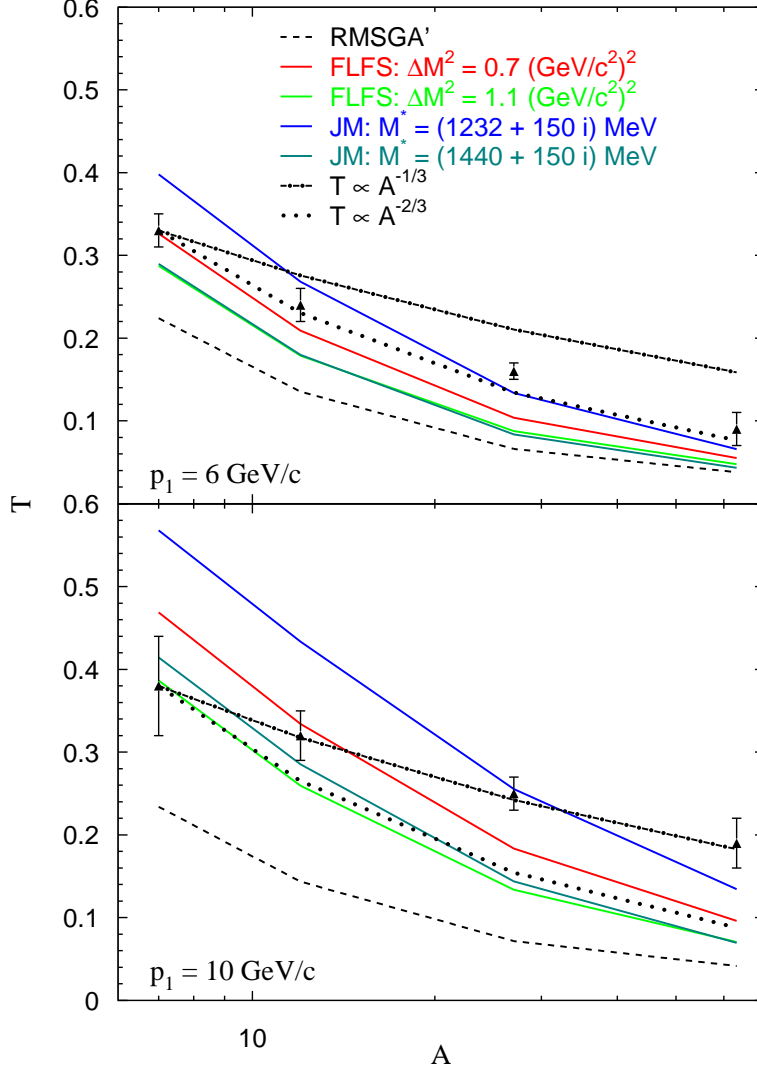


Fig. 4.  $A$  dependence of the nuclear transparency at two values of the incoming lab momentum  $p_1$ . The standard RMSGA calculations are represented by dashed curves, while the solid curves are RMSGA+CT+NF calculations with the positive sign for  $\phi(s) + \delta_1$ . The solid curves correspond with different descriptions of the CT effects, as indicated by the legend. The dot-dashed (dotted) curves display the  $A^{-1/3}$  ( $A^{-2/3}$ ) parametrization, normalized to the  ${}^7\text{Li}$  data points. Data are from Ref. [4].